Journal of Building Performance Simulation
Publication details, including instructions for authors and subscription information:
http://www.tandfonline.com/loi/tbps20

Comparing vertical ground heat exchanger models

Stephane Bertagnolio [a], Michel Bernier [b] & Michaël Kummert [b]

[a] Thermodynamics Laboratory, Universite de Liège, Sart Tilman Campus, B49-P33, Liege, 4000, Belgium

[b] Department of Mechanical Engineering, Ecole Polytechnique de Montreal, C.P. 6079, Succ. Centre-ville, Montreal, Quebec, H3C 3A7, Canada

Available online: 06 Feb 2012

To cite this article: Stephane Bertagnolio, Michel Bernier & Michaël Kummert (2012): Comparing vertical ground heat exchanger models, Journal of Building Performance Simulation, DOI:10.1080/19401493.2011.652175

To link to this article: http://dx.doi.org/10.1080/19401493.2011.652175

Journal of Building Performance Simulation
2012, 1–15, i*First* article

Taylor & Francis
Taylor & Francis Group

Comparing vertical ground heat exchanger models

Stephane Bertagnolio[a], Michel Bernier[b]* and Michaël Kummert[b]

[a]*Thermodynamics Laboratory, Universite de Liège, Sart Tilman Campus, B49-P33, Liege 4000, Belgium;* [b]*Department of Mechanical Engineering, Ecole Polytechnique de Montreal, C.P. 6079, Succ. Centre-ville, Montreal, Quebec H3C 3A7, Canada*

(*Received 4 May 2011; final version received 18 December 2011*)

The main objective of this article is to establish a set of test cases for analytical verification and inter-model comparison of vertical ground heat exchanger (GHX) models used in building simulation programs. Several test cases are suggested. They range from steady-state heat rejection in a single borehole to varying hourly loads with relatively large yearly thermal imbalance in multiple borehole configurations. The usefulness of the proposed test cases is illustrated with different GHX models. This comparison exercise has shown that analytical one-dimensional (1D) models compare favourably well with three-dimensional (3D) models for relatively short-simulation periods, where axial effects are not significant. Cyclic heat rejection/collection tests proved to be useful to characterize the accuracy and the computational performance of different load aggregation algorithms. Finally, different spatial superposition methods have been compared for various bore field sizes and configurations and various loads.

Keywords: modelling; ground heat exchanger; simulations; boreholes; heat pumps

1. Introduction

Closed-loop ground-coupled heat pump (GCHP) systems are now routinely installed to provide space conditioning in a wide range of applications from small residences to large commercial buildings. A schematic representation of such a system is shown in Figure 1. The operation of the system is relatively simple: a pump circulates a heat transfer fluid in a closed circuit from the ground heat exchanger (GHX) to heat pumps.

Typically, a vertical GHX consists of boreholes that are approximately 100 m deep with a 10–15 cm diameter. The number of boreholes in a bore field can range from one for a residence to several dozen in commercial applications. As shown in Figure 1, one or two U-tubes are usually inserted in boreholes, with fluid going down in one pipe (or two in the case of a double U-tubes configuration) and up the other(s). The volume between these pipes and the borehole wall is usually filled with grout to enhance heat transfer from the fluid to the ground and protect the aquifer.

In heating mode, the GHX acts as a heat source and heat is first transferred from the ground to the fluid loop and then to the evaporator side of the heat pumps before being released in the building. Assuming that there are no heat losses from the fluid loop, the total amount of energy transferred from the fluid loop to the heat pumps (Σq_i in Figure 1) is equal to the amount of heat extracted from the ground. In cooling mode, heat pumps transfer heat from the building to the fluid loop and the GHX is now a heat sink.

For a given borehole geometry, the average temperature level in the fluid loop depends mainly on four factors: the cumulative amount of heat collected (rejected) into the ground and the corresponding history (time sequence of heat collection/rejection), the far field ground temperature, T_g, the effective thermal resistance between the fluid and borehole wall temperatures and, of course, ground properties.

The precise evaluation of the annual heat pump energy consumption is intimately linked to the time-varying fluid temperature prediction. Ground loop temperature influences both the coefficient of performance (COP) and the capacity of the heat pump in both heating and cooling modes. Figure 2 shows the heating and cooling COP for typical heat pumps as a function of entering water temperature (EWT) – the EWT is equivalent to $T_{\text{out,ground}}$ shown in Figure 1 if piping losses are neglected. The slope of the COP curves is $+0.061/^{\circ}\text{C}$ and $-0.117/^{\circ}\text{C}$ for heating and cooling, respectively (Bernier 2006). Thus, for each 1°C variation in EWT, the COP will increase by 0.061 and decrease by 0.117 in heating and cooling, respectively. Also, shown in Figure 2 are curves representing the relative COP variation for an increase of 1°C of the EWT. For example, for EWT = 10°C, a 1°C increase in EWT leads to a COP increase of 1.49% in heating mode. The COP variations for heating and cooling

*Corresponding author. Email: michel.bernier@polymtl.ca

ISSN 1940-1493 print/ISSN 1940-1507 online

http://dx.doi.org/10.1080/19401493.2011.652175
http://www.tandfonline.com

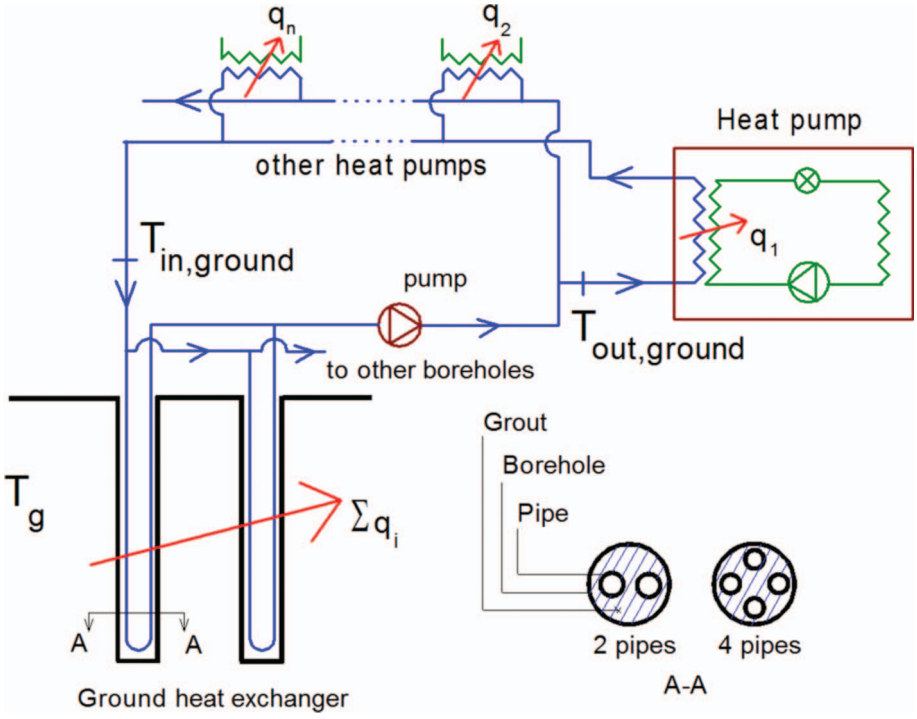

Figure 1. Typical closed-loop ground-coupled heat pump system.

have opposite signs. Thus, when a GHX model over predicts the EWT, the heat pump energy consumption will be under predicted in heating and over predicted in cooling. Conversely, the heat pump energy consumption will be over predicted in heating and under predicted in cooling, when the EWT is lower than the real value. The impact of an over- (or under-) prediction on annual heat pump energy consumption depends on the number of hours of operation in heating and cooling. Bernier *et al*. (2007) report that a uniform annual over-prediction of 2°C of the EWT can lead to a 6.5% error in the annual energy consumption for a heat pump operating in cooling for 2500 h per year.

GHXs models are usually composed of two sub-models representing two different regions: the first one is confined to the borehole itself (i.e. from the fluid to the borehole wall) and the second covers the zone from the borehole wall to the far field. Ground sub-models (or GHX models) are the main focus of the present investigation. Borehole sub-models, which essentially evaluate the borehole thermal resistance between the fluid and the borehole wall, are not investigated.

2. Objective

The main objective of this article is to establish a set of test cases for analytical verifications and inter-model comparisons of vertical GHX models used in building simulation programs. Several test cases are suggested. The cases range from steady-state heat rejection in a single borehole to varying hourly loads with large yearly thermal imbalance in multiple borehole configurations. The usefulness of the proposed test cases is illustrated with different GHX models. As expected, the applications of these cases reveal differences among models. However, it is outside the scope of this article to examine the exact causes of these differences. Based on the established BESTEST (Judkoff and Neymark 1995) terminology, the tests presented here fall into the categories of 'analytical verification' and 'comparative testing'.

3. Literature review

The following review surveys the literature for studies on GHX models comparison and validation. Bore field sizing programs and detailed hourly simulations of GHXs have two different objectives. In the former case, the overall required length is calculated based on expected ground loads and maximum temperature levels tolerated by the heat pumps. In the latter case, the length is known and $T_{out,ground}$ is the required output (usually at 1 h time intervals). Despite these different objectives, both approaches use similar techniques to model ground heat transfer.

Sizing software packages for GHX have been compared for residential and commercial applications.

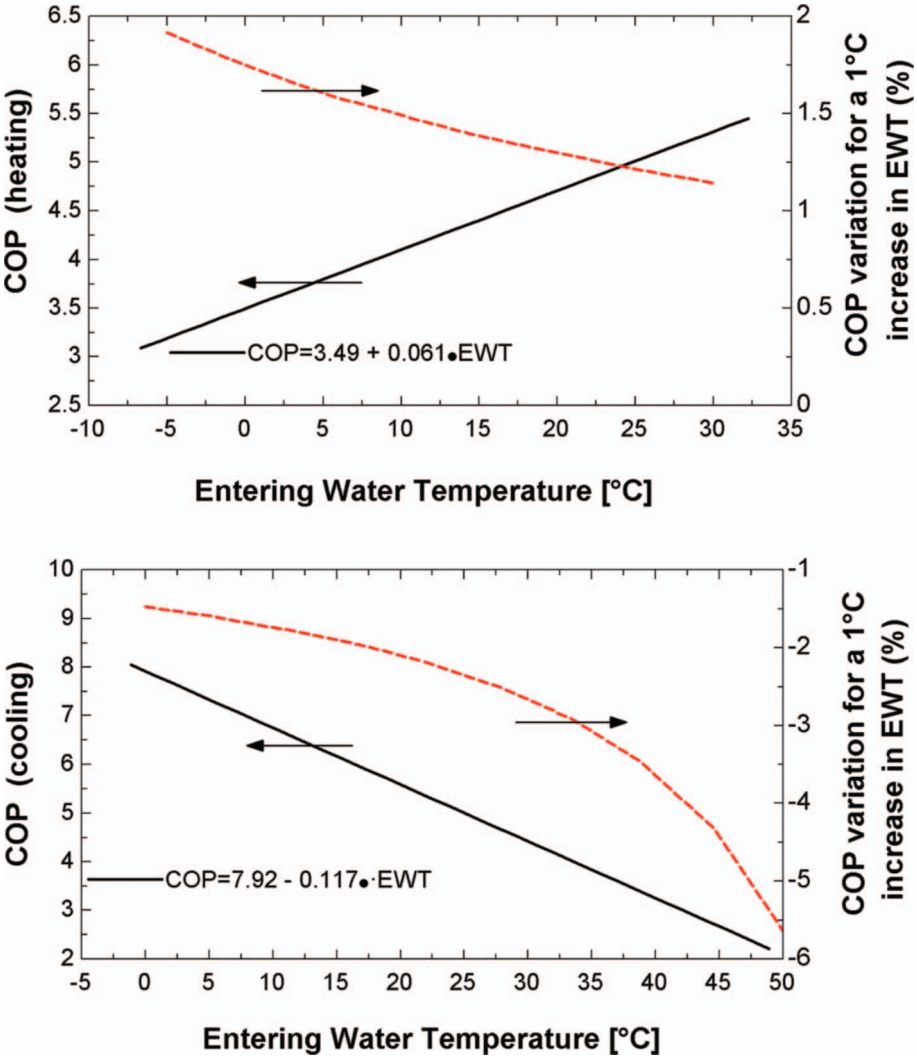

Figure 2. Average COP values as a function of the heat pump entering water temperature (EWT).

In the case of residential applications, Shonder *et al.* (1999) examined two cases for heating-dominated and cooling-dominated climates. The authors show that the GHX length predicted by six different sizing programs are within $\pm 7\%$ and $\pm 16\%$ of each other for these two cases. Comparison was also made with the duct storage (DST) model (Hellström *et al.* 1996) which was referenced by the authors as being the 'benchmark'. Shonder *et al.* (2000) also used the DST benchmark in their comparison for larger commercial applications. They compared four sizing programs. Three of these programs agree with the benchmark lengths to within $\pm 12\%$.

Validations or comparisons of GHX models used in hourly simulation programs have been performed on a limited basis. In his pioneering work, Eskilson (1987) showed that his *g-functions* were in good agreement with the well-known line-source analytical solution (Carslaw and Jaeger 1947, Ingersol *et al.* 1954). However, this comparison was limited to constant heat rejection. Yavuzturk and Spitler (1999) extended the work of Eskilson to short-time steps. They compared their model with an experimental data set and showed good agreement (Yavuzturk and Spitler 2001). Fisher *et al.* (2006) compared the short-time step model with Hellström's (1991) line-source model for a composite heat collection function. The maximum difference (1.7°C) between the two approaches occurred when a pulse load was periodically applied. They also compared their results with experimental data from Hern (2002). This comparison included the GHX model as well as the heat pump model. The resulting system model predicted ground heat transfer rate to within 6% of the experimental results.

Huber and Pahud (1999) ran a series of 20 test cases to compare two models. Their tests covered

several operating conditions and bore field geometries. Their inter-model comparison proved to be helpful in revealing differences in the models.

Bernier *et al.* (2004) have compared their GHX model with the DST model. They note that both models are in good agreement. However, extensive testing was not performed. More recently, Spitler *et al.* (2009) have carried out a comparison of GHX models for two typical installations: a three-borehole system installed at Oklahoma State University for which experimental data are available for a 15-month period and a 196-borehole installation serving an office building for which only simulation results are considered. Six models were compared and significant differences in the prediction of the GHX outlet fluid temperature are reported but no indications are given on the sources of these discrepancies.

Philippe *et al.* (2009) examined the validity range of three analytical solutions to the problem of transient conduction in the ground for single boreholes: the one-dimensional (1D) infinite line-source (ILS) model, the 1D infinite cylindrical heat source (CHS) model and the two-dimensional (2D) finite line-source (FLS) model. For short simulations (less than a few days), axial conduction can be neglected and the authors recommended the CHS. For longer simulations (a few months to several years), axial effects become important and the FLS model is recommended. Between these two limits, the ILS can be used with good accuracy. No comparison of load aggregation and spatial superposition techniques has been provided in this last study.

Another validation method for GHX models consists in using data obtained from experimental tests conducted with laboratory sand box rigs. Yu *et al.* (2008) have conducted such tests to validate a detailed mathematical model for ground heat transfer including ground freezing. Beier *et al.* (2011) have also applied the sand box method and provide experimental data allowing verification of GHX models and thermal response tests (TRT) procedures. The usefulness of the provided set of data has been illustrated with three different GHX models.

4. Bore field geometry

Figure 3 shows a typical 4×4 bore field and the nomenclature that will be used in this article. The depth is H and the active heat exchange area typically starts at a distance D from the ground surface, while B is the centre-to-centre borehole spacing. The ground is characterized by its thermal conductivity, k_g, thermal diffusivity, α_g, and by the undisturbed ground temperature, T_g. As shown in Figure 3, the borehole fluid loops are usually connected in parallel in a reverse-return circuit ensuring that each borehole receives an equal share of the total flow rate, $\dot{m}_{\text{total}}$. The inlet temperature to each borehole is equal to the return temperature from the heat pumps, $T_{\text{in,ground}}$. The outlet temperature from the bore field, $T_{\text{out,ground}}$, represents the average borehole outlet temperature.

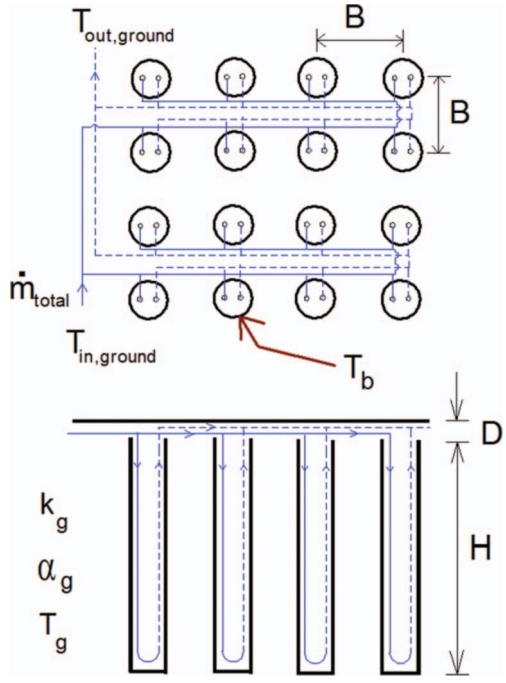

Figure 3. Typical bore field geometry.

In the following sections, the parameter q is used to represent the amount of heat rejected/collected per unit length. The convention used here is that a negative values of q corresponds to heat rejection into the ground. It should not be confused with the total heat rejected/collected into the ground (Σq_i in Figure 1).

5. Review of GHX models

Following is a brief description of some ground sub-models available in the literature. These models were chosen as candidates to evaluate the proposed test cases. All models assume that heat transfer is by pure conduction only. Models that couple heat and moisture transfer in the ground (e.g. Tarnawski and Leong 1993, Reuss *et al.* 1997, Piechowski 1998) will not be covered in this study. This selection was based on two criteria. First, these models were readily available to the authors. Second, these models are significantly different in their treatment of ground heat transfer, thermal interaction among boreholes and load aggregation. Therefore, they offer a wide range of possibilities to evaluate the relevancy of test cases.

These models are divided into two categories: analytical and numerical/hybrid models.

5.1. Analytical models

5.1.1. Infinite line source (ILS)

The 1D ILS model is an application of Lord Kelvin's line source to ground exchangers (Kelvin *et al.* 1882). The heat transfer rate per unit length is applied to an infinitely long line. The solution provides temperature at various radial distances. A curve fit of the tabulated values provided by Ingersoll and Plass (1948) is used here.

5.1.2. Cylindrical heat source (CHS)

The CHS model was first introduced by Carslaw and Jaeger (1947) and later developed by Ingersoll *et al.* (1954). This method uses an analytical solution for 1D radial heat conduction from a cylinder subjected to a constant heat flux at its periphery. The solution proposed by Cooper (1976) to obtain the temperature at the cylinder periphery is used in the present work. Like the other analytical methods, the CHS solution can be used with time-varying heat rejection by using the principle of temporal superposition (Bernier 2001).

5.1.3. Finite line source (FLS)

The FLS method was proposed by Eskilson (1987) and detailed by Zeng *et al.* (2002). This model assumes that the heat transfer rate per unit length is applied to a finite length line corresponding to the axis of the borehole. It provides 2D (radial and axial) temperatures in the ground including the borehole wall. In the present work, the average borehole wall temperature is used. It is obtained by integrating the FLS equation over the borehole height. More recently, Cui *et al.* (2006) have proposed a new formulation of the FLS method for inclined boreholes allowing the simulation of bore fields composed of vertical and inclined boreholes.

5.2. Numerical/hybrid models

5.2.1. g-functions

Eskilson (1987) has shown that, for a fixed value of header depth ($D = 4$ or 5 m in his study), the thermal response of a bore field is a function of three non-dimensional parameters: B/H, the bore field aspect ratio; r_b/H, the non-dimensional borehole radius and t/t_s, a non-dimensional time, where t_s is a characteristic time $= (H^2/9\alpha_g)$. Eskilson shows that the borehole wall temperature (T_b in Figure 3) is given by:

$$T_b = T_g - \frac{q}{2\pi k_g} \times g(t/t_s, r_b/H, B/H) \qquad (1)$$

where 'g' represents Eskilson's *g-functions*. These *g-functions* have been generated using 2D numerical simulations combined with spatial superposition to effectively obtain a three-dimensional (3D) response of the bore field. It is important to note that the *g-functions* were derived using a uniform borehole wall temperature (T_b) for every borehole in the bore field in order to approximate typical field conditions, where every borehole is supplied with the same inlet fluid temperature. Consequently, the 'specific' heat transfer rates of every borehole are different and vary with time but the global heat transfer rate for the bore field (q) is constant. A number of *g-functions* for several configurations are available in Eskilson's thesis (Eskilson 1987). They are presented graphically as a function of $\ln(t/t_s)$ for a particular bore field geometry (B/H) and for a given value of r_b/H. In the present work, the *g-functions* have been obtained by digitizing the curves provided in Eskilson's original thesis. The response to any heat rejection/collection value of q can be determined by dividing the heat rejection/collection into a series of step functions and superimposing the response to each step function. However, for a typical borehole, the original *g-functions* are valid for times larger than 3–6 h and so cannot be used for short-time steps simulations (1 h and below) which are usually encountered in annual simulations.

Yavuzturk and Spitler (1999) have extended the application of Eskilson's *g-functions* to simulations with time steps between 2.5 min and 200 h. The resulting short-time step *g-functions* have been generated by means of a 2D numerical model which incorporates the borehole content thus combining borehole and ground sub-models into one. In order to reduce the computational time, an aggregation algorithm is proposed. Because their influence diminishes with time, past loads are aggregated together in blocks of 730-h time periods and superposed to more recent loads. As shown in Figure 4, a minimum hourly history period of 192 h of non-aggregated loads is suggested by the authors to avoid any abrupt transition between recent loads and past aggregated loads. During simulation, a new average block is created as soon as a new period of 922 (730+192) h has ended. This aggregation algorithm, referred to '730-block', will be used later in conjunction with the CHS model.

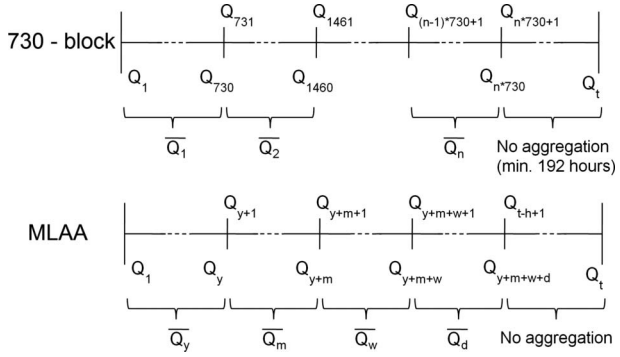

Figure 4. '730-block' and 'MLAA' aggregation algorithms.

5.2.2. *Hybrid CHS/T_p/MLAA*

Bernier *et al.* (2004) proposed a hybrid model, where local effects in the ground at the borehole level are calculated using the CHS model and borehole thermal interference is evaluated numerically. They extended the aggregation scheme of Yavuzturk and Spitler (1999) into several aggregation periods of varying sizes. This so-called multiple load aggregation algorithm (MLAA) is presented schematically in Figure 4.

This results in the following relationship for the borehole wall temperature at time t:

$$T_{b,t} = T_g + T_{p,t} - \frac{1}{k_s H}(\mathrm{MLAA})$$

$$\begin{aligned}\mathrm{MLAA} = {} & \overline{Q_y} \times [G(\mathrm{Fo}_{t=t}) - G(\mathrm{Fo}_{t=t-y})] \\ & + \overline{Q_m} \times [G(\mathrm{Fo}_{t=t-y}) - G(\mathrm{Fo}_{t=t-y-m})] \\ & + \overline{Q_w} \times [G(\mathrm{Fo}_{t=t-y}) - G(\mathrm{Fo}_{t=t-y-m-w})] \\ & + \overline{Q_d} \times [G(\mathrm{Fo}_{t=t-y-m-w}) - G(\mathrm{Fo}_{t=h})] \\ & + Q_{t-h} \times [G(\mathrm{Fo}_{t=h}) - G(\mathrm{Fo}_{t=h-1})] + \cdots \\ & + Q_{t-1} \times [G(\mathrm{Fo}_{t=2}) - G(\mathrm{Fo}_{t=1})] \\ & + Q_t \times G(\mathrm{Fo}_{t=1}) \end{aligned} \quad (2)$$

where T_g is the far-field temperature, $T_{p,t}$ is a temperature penalty at time t which accounts for thermal interaction among boreholes, G is the CHS solution and Fo ($=4\alpha t/d^2$) is the Fourier number evaluated for various times t. Values of $\overline{Q}$ represent average ground loads over each aggregation period. In the original work of Bernier *et al.* (2004), $T_{p,t}$ was evaluated using a 2D numerical model. More recently, Bernier *et al.* (2008) used thermal response factors to obtain the average temperature increase (decrease) at the borehole wall caused by the thermal interaction from the other boreholes. The thermal response factors are generated by means of the original *g-functions* provided by Eskilson (1987). The MLAA term on the right hand side of Equation (2) accounts for heat transfer at the borehole level (excluding borehole interaction). This term represents the difference between the borehole wall temperature and the undisturbed ground temperature. This difference is evaluated using the CHS model. The MLAA uses two major thermal history periods, referred to as 'past' and 'immediate'. The immediate thermal history (h) is not aggregated, while the past thermal history is subdivided into four time intervals with periods of the order of a day (d), a week (w), a month (m) and years (y) (Bernier *et al.* 2004). Results presented here were obtained with h, d, w and m equal to 24, 48, 168 and 360 h, respectively.

5.2.3. *DST model*

Hellström (1991) developed a 3D simulation model for seasonal thermal energy storage with vertical GHXs. The model incorporates the spatial superposition of three parts: a so-called 'global' temperature difference between the heat store volume and the undisturbed ground temperature, a temperature difference from the 'local' solution around the heat store volume and a temperature difference from the 'local' steady-flux part. The model was implemented in the TRNSYS (Klein 2006) simulation program by Hellström *et al.* (1996). As explained by Chapuis and Bernier (2009), the DST model implemented in TRNSYS assumes that the boreholes are placed uniformly within a cylindrical storage volume of ground. The user specifies the desired spacing between boreholes and the program calculates the corresponding storage volume using Equation (3). Thus, the user is not allowed to specify a rectangular geometry such as the one presented in Figure 3.

$$V_{\mathrm{DST}} = \pi \times n \times H \times (0.525 \times B)^2. \quad (3)$$

6. Overview of the proposed test cases

GHX models differ in the way they calculate local (near the borehole) heat transfer, thermal interaction among boreholes and load aggregation. Therefore, test cases need to evaluate models in at least these three areas.

This section provides an overview of the proposed test cases, further details are provided in the results section. The test cases range from steady-state heat rejection in a single borehole to varying hourly loads with relatively large yearly thermal imbalance in multiple borehole configurations. All tests performed in the present study are summarized in Table 1, where 'SB' stands for 'single borehole' tests and 'MB' stands for 'multiple boreholes' bore fields with 2, 8 or 64 boreholes. The letters A, B, C and D represent various load profiles: A: constant heat load, B: 12 or 24 h

Table 1. Summary of test cases.

Case	Bore field configuration	Load profile	Normalized load ($q/2\pi k_g$ in°C)	Borehole depth (m)	Borehole radius (m)	Header depth (m)	Undisturbed ground temperature (°C)	Ground conductivity (W/m-K)	Ground diffusivity (m^2/day)	Borehole distance (m)	DST storage volume (m^3)	Comments	Models
SB-A	1 × 1	Constant heat rejection	−1	110	0.055	5	0	1.3	0.0624	–	2381	Base case for analytical verification (single borehole)	CHS, ILS, FLS, *g-function*, DST
SB-B12	1 × 1	Periodic symmetric load (12 h period)	−1/+1	110	0.055	5	0	1.3	0.0624	–	2381	Comparison of load aggregation algorithms (single borehole)	CHS, ILS, CHS-MLAA, CHS-730, DST
SB-B24	1 × 1	Periodic symmetric load (24 h period)	−1/+1	110	0.055	5	0	1.3	0.0624	–	2381	Comparison of load aggregation algorithms (single borehole)	CHS, ILS, CHS-MLAA, CHS-730, DST
SB-C	1 × 1	Synthetic asymmetric load (cooling dominated)	−5.42/2.81	110	0.055	5	0	1.3	0.0624	–	2381	Realistic load profile (single borehole)	CHS-MLAA, CHS-730, DST
SB-D	1 × 1	Heat collection only	0/5.42	110	0.055	5	0	1.3	0.0624	–	2381	Realistic load profile (heating only, single borehole)	CHS-MLAA, CHS-730, DST
MB2-A	2 × 1	Constant heat rejection	−1	110	0.055	5	0	1.3	0.0624	5.5	5763	Evaluation of thermal interactions between boreholes (base case)	*g-function*, DST, hybrid CHS/T_p/MLAA
MB8-A	8 × 1	Constant heat rejection	−1	110	0.055	5	0	1.3	0.0624	5.5	23050	Evaluation of thermal interactions between boreholes (elongated borefield)	*g-function*, DST, hybrid CHS/T_p/MLAA
MB64-A	8 × 8	Constant heat rejection	−1	110	0.055	5	0	1.3	0.0624	5.5	184402	Evaluation of thermal interactions between boreholes (rectangular borefield)	*g-function*, DST, hybrid CHS/T_p/MLAA
MB64-C	8 × 8	Synthetic asymmetric load (cooling dominated)	−5.42/2.81	110	0.055	5	0	1.3	0.0624	5.5	184402	Realistic load profile (multiple boreholes)	DST, hybrid CHS/T_p/MLAA

period symmetric heat load, C: asymmetric load (cooling dominated) and D: heating only load. Analytical solutions (CHS, ILS and FLS) without aggregation and spatial superposition capabilities have only been tested for SB cases, since they are unable to simulate the thermal behaviour of bore fields. The 'MLAA' and '730-block' aggregation algorithms have been coupled to the same analytical function (CHS) and run with different variable load profiles to allow comparison in SB test cases. Eskilson's *g-functions* have been tested with constant heat load profiles only. The DST model, implemented in TRNSYS, is used in every test case. The hybrid CHS/T_p/MLAA model is used in multiple boreholes tests only. All tests are performed with a 1-h time step. Finally, for the case of the DST model, the value of the borehole resistance is set to a very small value and the flow rate to a high value so that the mean fluid temperature can be assumed to be equal to the borehole wall temperature.

7. Results

7.1. Single borehole

7.1.1. Constant heat rejection

This test consists of rejecting a constant amount of heat into the ground and calculating the resulting variation of the borehole wall temperature with time. This is the most basic test case. It can be considered to be an analytical verification of the *g-function* and DST models with the CHS, ILS and FLS analytical solutions. Since the ground load is constant, temporal superposition and load aggregation are not tested. Furthermore, for a single borehole, thermal interaction is not an issue. The various parameters used for this test, which will be referred to the SB-A test, are given in Table 2. Note that T_g and the ratio $q/2\pi k_g$ have been conveniently set to 0°C and −1°C, respectively. Thus, according to Equation (1), T_b corresponds directly to the value of the *g-function* (see Equation (1)). A different set of ground properties has been used for the DST than for the other four models. This was done to limit the calculation time of the DST model which can be relatively large considering that large values of $\ln(t/t_s)$ may translate into hundreds of years of simulations for typical ground characteristics.

Figure 5 presents a comparison of the borehole wall temperature predicted by the five models for this test case. Since heat rejection is constant, it is convenient to present the results as a function of non-dimensional time, $\ln(t/t_s)$ (recall that t_s is the characteristics time defined by $H^2/9\alpha$). Furthermore, with $T_g = 0$°C, the borehole wall temperature is directly proportional to the ratio $q/2\pi k_g$. For reference, with a ground thermal diffusivity of 0.0624 m^2/day and

Table 2. Parameters used for the single borehole constant heat rejection case (SB-A).

Parameter		DST	CHS, ILS, FLS, *g-function*
Borehole depth	H	110 m	110 m
Borehole radius	r_b	0.055 m	0.055 m
Borehole header depth	D	5 m	5 m
Undisturbed ground temperature	T_g	0°C	0°C
Ground thermal conductivity	k_g	1.3 W/m-K	3.5 W/m-K
Ground thermal diffusivity	α	0.0624 m^2/day	0.14 m^2/day
Ground load (expressed in terms of temperature)	$q/2\pi k_g$	−1°C	−1°C
Storage volume (DST only)	V_{DST}	2381 m^3	–

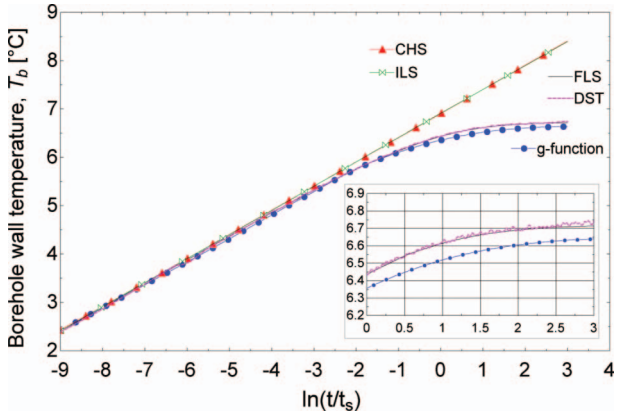

Figure 5. Results of the SB-A test case.

the data listed in Table 2, values of $\ln(t/t_s)$ of −9, −1.08 and 0 correspond to periods of 64 h, 20 years and 59 years after the start of the heat rejection, respectively. As shown in this figure, the CHS and ILS models give almost identical results. Similarly, the *g-function*, FLS and DST models follow very similar trends. However, both group of models start to differ from each other when ln (t/t_s) reaches a value of approximately −3. The difference is around 0.13°C after 5.9 years, 0.3°C after 20 years and reaches 0.55°C after 59 years.

One possible cause of this difference stems from the fact that after a certain time, axial heat transfer in the ground becomes important. Axial heat transfer tends to slow the rate of increase of borehole wall temperature with time up to a point, at steady-state, where the heat injected in the borehole equals the heat transferred through the ground surface. Since the CHS

and the ILS are 1D radial models, it is not surprising to see a constant rate of increase of borehole wall temperature and that the difference in borehole wall temperature becomes important at steady-state. It is also interesting to note that the *g-function*, the FLS and the DST models tend to reach a steady-state as evidenced by the plateau in the borehole wall temperature reached by these models for $\ln(t/t_s) > 3$.

The difference between the DST and FLS models is very small with an RMS error of about 0.02 K. However, the difference between these two models and the *g-function* is larger, especially for large values of $\ln(t/t_s)$ (i.e. long simulation periods) as shown in the inset in Figure 5 (the difference is approximately 0.1 K for $\ln(t/t_s) = 3$ or $t = 528$ years). The exact cause of this difference is unknown; a closer look at how the borehole wall temperature is evaluated by the DST model might provide an answer.

7.1.2. *Symmetric cyclic heat rejection/collection*

This test, named SB-B, consists of imposing constant and symmetric cycles of heat rejection/collection. As shown in Table 3, values of $q/2\pi k_g$ which alternate from $+1^\circ$C to -1°C each 12 or 24 h have been selected. This test is used to compare the various load aggregation schemes and short-time step capabilities of the various models. Figures 6 and 7 show the results obtained for the last week in a 10-week test.

A first test has been performed using a 12-h period load variation in order to assess short-time step capabilities. The results are shown in Figure 6: the bottom part of the figure shows the borehole temperature and the top part shows the difference between selected models. The results confirm the analysis made by Philippe *et al.* (2009): the deviation of the ILS from the more accurate solution given by the CHS decreases to approximately 10% when the Eskilson criteria ($\mathrm{Fo} = 4\alpha t/d^2 > 5$) is satisfied. In the present case, this corresponds to approximately 6 h after a sudden change in heat rejection/collection. A smaller difference can also be observed between the DST and CHS models. This difference is around 0.3 K 1 h after a sudden change and it is virtually null after 12 h.

As shown in Figure 7, the results for the CHS-no aggregation, CHS-730 and DST models are almost indistinguishable. The CHS-MLAA follows the other three models except near the changeover from heating to cooling and vice versa. This is due to the load aggregation scheme of the CHS-MLAA which averages loads that are not part of the immediate (last 24 h) thermal history. However, RMS deviations for the whole week between the models and the non-aggregated CHS solution are all of the same order of magnitude (between 0.024 for the CHS-730 and 0.089 K for the CHS-MLAA) and all four models provide results within ± 0.3 K. Extending the hourly history period of the CHS-MLAA algorithm from 24 to 48 h (not shown in Figure 7) reduces the RMS deviation between this model and the non-aggregated CHS solution from 0.089 to 0.048 K. It is interesting to note that the computational times of the aggregated schemes are much lower than the CHS-no aggregation scheme. For a one-year simulation, the computation time for the CHS-730 and the CHS-MLAA are 88% and 99.3% lower than for the CHS-no aggregation scheme. These results confirm that aggregation introduces a small error in the evaluation of the borehole

Table 3. Parameters used for the cyclic heat rejection/collection case (SB-B).

Parameter		Value
Borehole depth	H	110 m
Borehole radius	r_b	0.055 m
Borehole header depth	D	5 m
Undisturbed ground temperature	T_g	0°C
Ground thermal conductivity	k_g	1.3 W/m-K
Ground thermal diffusivity	α_g	0.0624 m^2/day
Load	$q/2\pi k_g$	Cycle of $+1^\circ$C for 12/24 h then -1°C for 12/24 h

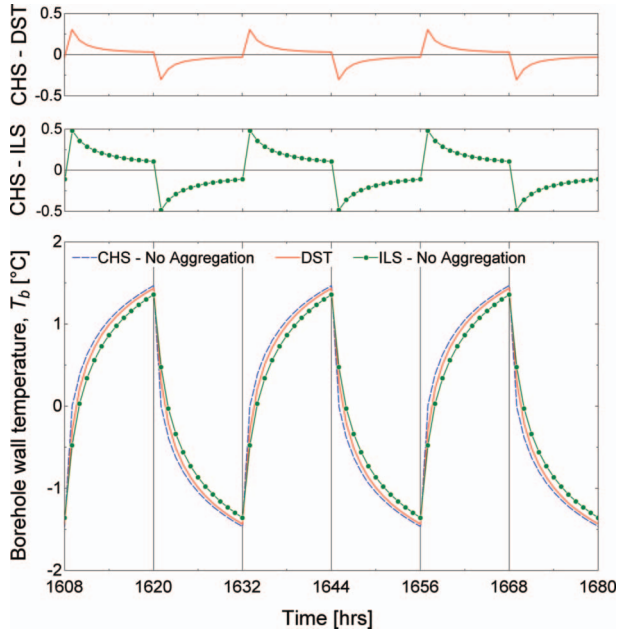

Figure 6. Comparison of three models for the SB-B test case with a 12-h period cyclic load.

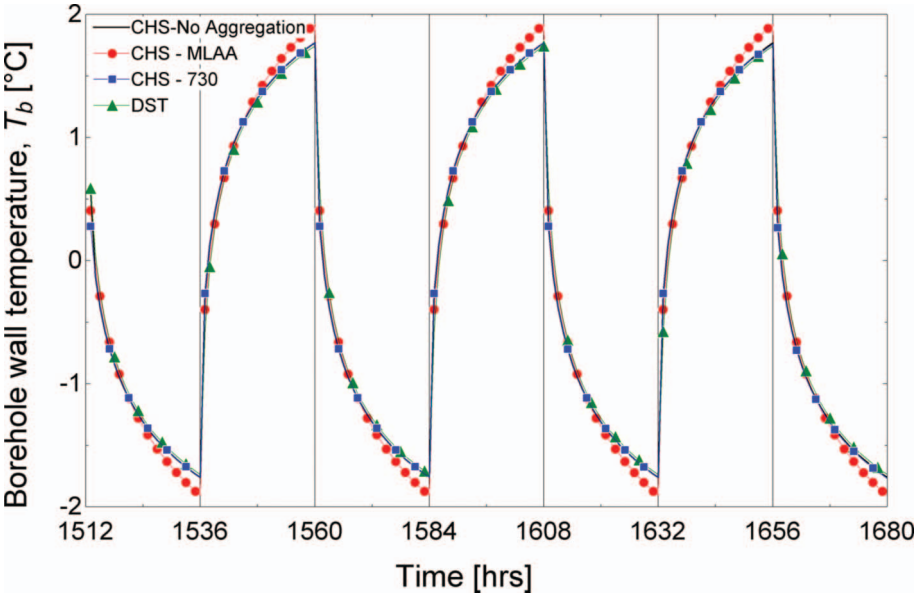

Figure 7. Comparison of four models for the SB-B test case with a 24-h period cyclic load.

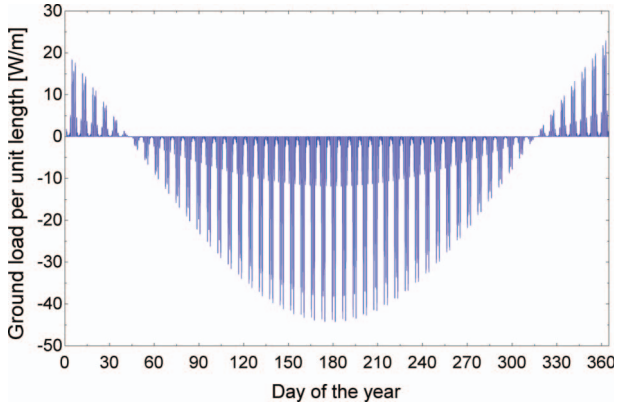

Figure 8. Synthetic asymmetric load profile.

wall temperature but makes the calculations significantly faster.

7.1.3. *Synthetic asymmetric load profile*

The SB-C test consists of calculating the resulting borehole wall temperature over long periods when the borehole is subjected to an asymmetric load profile. This load profile is generated using a mathematical function (Bernier *et al.* 2004) which is described in Appendix 1. The resulting load profile is shown in Figure 8, where negative values indicate heat rejection into the ground. This profile emulates a cooling-dominated load. The average annual load is -2.83 W/m.

Simulations are performed with the CHS-MLAA, CHS-730 and DST models using this load profile and the parameters listed in Table 4. Results of the last year of a 20-year simulation are shown and analysed in Figure 9. As shown in the top portion of this figure, the DST and the CHS-MLAA models agree with each other within approximately ± 0.7 K and with a RMS of 0.26 K. The difference between the DST and the CHS-730 models is smaller and varies between ± 0.5 K with a RMS of 0.12 K. Thus, all three models seem to aggregate loads satisfactorily over a 20-year period. Similar simulations were performed with ground thermal conductivities of 2.2 W/m-K and 3.1 W/m-K (with corresponding ground thermal diffusivities of 0.101 and 0.144 m^2/day). These results (not shown here) show comparable differences between all three models. Finally, it is interesting to note that the 1D CHS model gives relatively similar results either with the 730 time blocks or the MLAA algorithm.

Table 4. Parameters used for cases SB-C and SB-D.

Parameter	Value
H	110 m
r_b	0.055 m
D	5 m
T_g	0°C
k_g	1.3
α_g	0.0624

7.1.4. *Synthetic non-continuous load profile*

This test, named SB-D, consists in calculating the temperature response of a single borehole for long-term simulations for a heating-only solicitation. This load profile is obtained by conserving only the positive

values of a symmetric load profile (see the Appendix 1 for more details). The resulting load profile is shown in Figure 10, where positive values indicate heat collection from the ground. The objective of this test case is to assess the temperature variation predicted by the models, especially the ones that use aggregation periods, after a long period (summer) without any ground thermal solicitation. The borehole and ground characteristics are the same as those used in previous test cases (Table 4).

Hourly simulations are performed for a 20-year period and the results of the 20th year are shown and analysed in Figure 11. Once again, when compared to the DST model, the difference with the CHS-730 algorithm is smaller than with the CHS-MLAA model. Overall, differences are relatively small and all the three models aggregate non-continuous loads satisfactorily with all results within a ± 0.6 K range and a maximum RMS of 0.2 K. The constant temperature profile given by the CHS-MLAA during the 'summer' period (when the load is equal to zero), while other models predict a slight temperature increase, is due to the specific aggregation method which is based on the use of 'floating' averages.

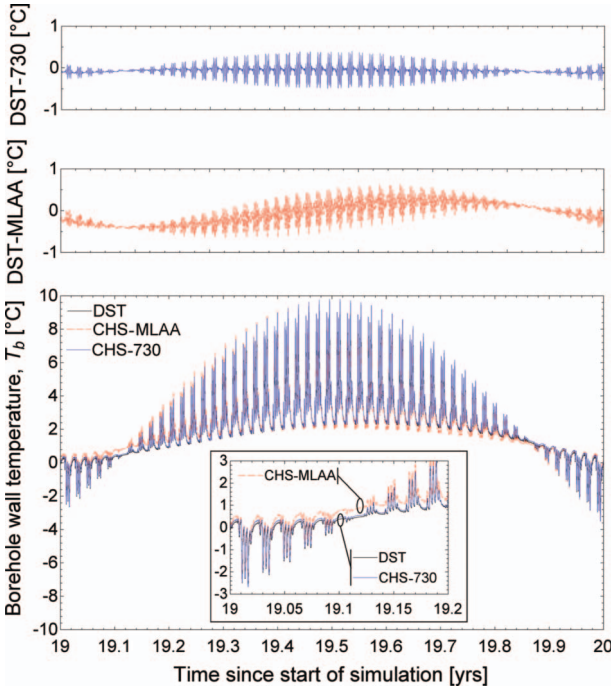

Figure 9. Comparison of the CHS-MLAA, CHS-730 and DST models for the SB-C test case.

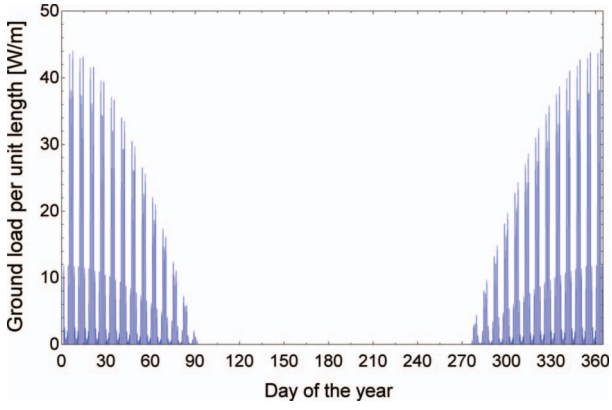

Figure 10. Synthetic non-continuous load profile.

7.2. *Multiple boreholes*

Aside from testing the local (at the borehole) heat transfer and load aggregation over time, multiple borehole tests add one more degree of complexity, i.e. thermal interaction among boreholes. Bore field configurations of 2, 8 (8×1) and 64 (8×8) boreholes with $B/H = 0.05$ are compared for two different test series. Only the DST, the *g-functions* and the hybrid CHS/T_p/MLAA models are considered for the following test cases.

7.2.1. *Constant heat rejection*

The MB-A test series uses the SB-A test parameters except that bore fields of 2, 8 and 64 boreholes are considered. Results are shown in Figures 12–14. For

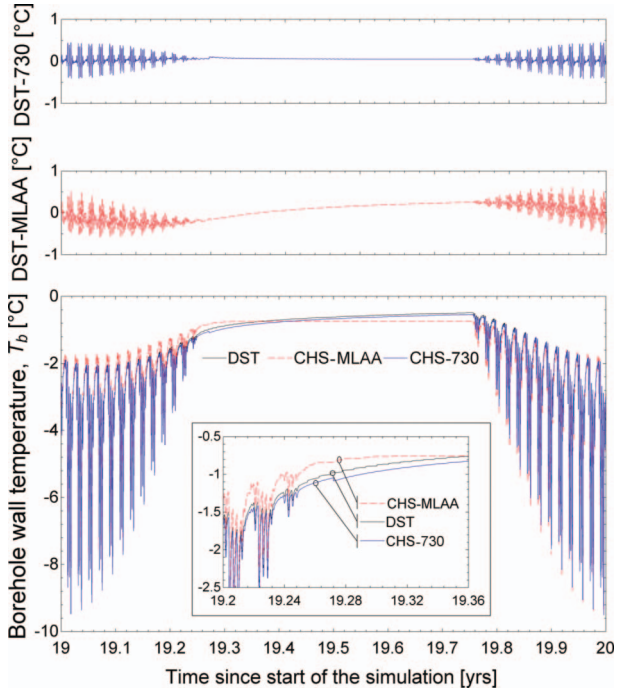

Figure 11. Comparison of the CHS-MLAA, CHS-730 and DST models for the SB-D test case.

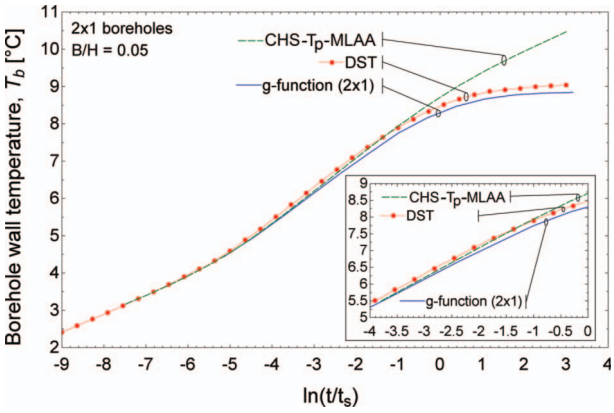

Figure 12. Test MB2-A for 2 boreholes.

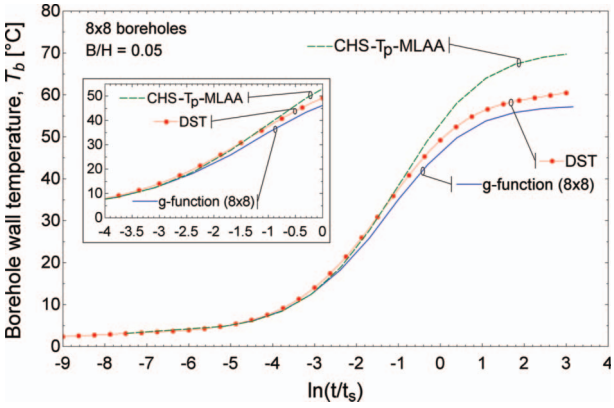

Figure 13. Test MB64-A for 64 boreholes.

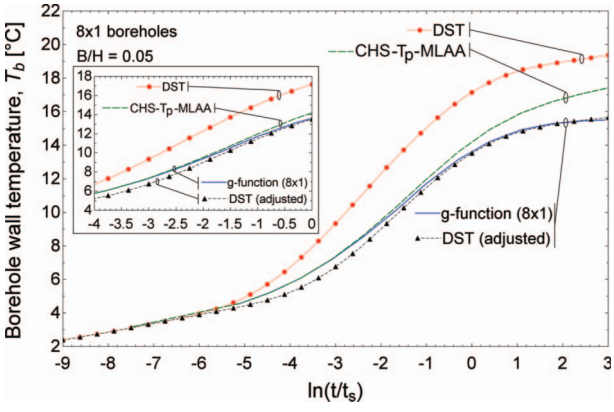

Figure 14. Test MB8-A for 8 boreholes.

the 2 borehole configuration (MB2-A test), a difference of 0.18°C is observed between the hybrid CHS/T_p/MLAA and the *g-function* models for $\ln(t/t_s) = -1.08$ (i.e. after a simulation time of 20 years). At the same time, the difference between the *g-function* and DST models is about 0.16°C. As was noted in relation to Figure 5, the DST model and the *g-function* tend to reach a steady-state condition, while the borehole wall temperature predicted by the hybrid CHS/T_p/MLAA model continues to rise as shown in Figure 12. As explained before, the solution given by the CHS at the borehole level does not consider axial heat transfer which becomes important for large simulation times. However, contrary to the behaviour observed for the single borehole, the temperature rise given by the hybrid CHS/T_p/MLAA model is not linear. This is due to the fact that T_p is calculated based on a 3D model thus accounting for axial heat transfer.

The results for the 64 boreholes (square 8 × 8 configuration, MB64-A) presented in Figure 13 reveal some significant differences among models. After 20 years ($\ln(t/t_s) = -1.08$), the difference between the hybrid CHS/T_p/MLAA and the *g-function* models is 3.09°C, while the *g-function* and DST models differ by 2.48°C for the same time period. The deviation between the DST model and the *g-function* can be partly explained by the cylindrical arrangement of the boreholes imposed in the DST model. Indeed, the 8 × 8 configuration bore field is simulated by the DST model as a cylindrical storage volume with boreholes placed axisymmetrically with a 5.5 m uniform spacing. The steady-state values (for $\ln(t/t_s) > 3$) are quite different with approximately a 13°C difference between the *g-function* and the hybrid CHS/T_p/MLAA models. Again this difference is probably attributable to the fact the CHS solution at the borehole level does not consider axial heat transfer. However, as noted in Figure 12, the borehole temperature rise is 'flattened' by T_p, the borehole thermal interaction. It has to be mentioned that computed values of temperature differences between models are also due to the large, non-realistic and temperature increases. For a practical heat pump application, the differences would be more modest.

A last test consists of comparing the same three models for an elongated 8 × 1 bore field (Figure 14, MB8-A test). For this test, the hybrid CHS/T_p/MLAA model follows Eskilson's *g-function* curve except for long-term periods when axial effects have a major impact. The effect of the particular (cylindrical) configuration imposed by the DST approach appears to be significant even for short periods and results in a significant deviation between the DST curve and the two others (2°C after only 2.94 years of simulation or $\ln(t/t_s) = -3$).

In an attempt to improve the DST model, adjustments were made to the storage volume. The initial storage volume of 23,050 m^3, obtained by means of Equation (3) for eight 110-m deep boreholes with a spacing of 5.5 m, was manually adjusted in order to fit the *g-function*. The best fit was obtained for a thermal

storage volume of 80,000 m^3. As shown in Figure 14, this modification reduces the difference between the DST and the *g-functions* to values below 0.6°C. It is interesting to note that the adjusted value of the thermal storage volume is quite similar to the value obtained with a cylinder (85,793 m^3) whose perimeter is given by $2 \times ([n \times B] + B)$. This can be explained by the fact that the heat exchanged between the storage volume and the surrounding (far-field) ground computed by the DST model is a function of the side area (and consequently of the perimeter) of the storage volume. This observation has not been verified for other cases and would deserve further investigation (with different geometries/configurations/loads/etc.) in order to draw more general conclusions on how to adjust the DST model for bore field patterns that differ from the assumed cylindrical geometries.

7.2.2. *Synthetic asymmetric load profile*

This test series, named MB-C, uses the same load profile utilized for test SB-C, including the asymmetric load profile shown in Figure 7. Tests for 64 boreholes (MB64-C) are presented in Figure 15 for the hybrid CHS/T_p/MLAA and DST models. The top portion of this figure indicates the difference between the DST and hybrid CHS/T_p/MLAA models. With such a dense bore field, heat gets trapped in middle boreholes which tend to raise the overall borehole wall temperature.

As shown in Figure 15, the CHS/T_p/MLAA model tends to slightly underestimate the borehole wall temperature compared to the DST model. This discrepancy is of the same order of the magnitude as the ones previously observed and is about 1.1°C after 20 years. This deviation results of the combination of the effects of the use of the load aggregation algorithm of CHS/T_p/MLAA model, of the cylindrical symmetry considered in the DST model and of the axial heat transfer neglected by the CHS model.

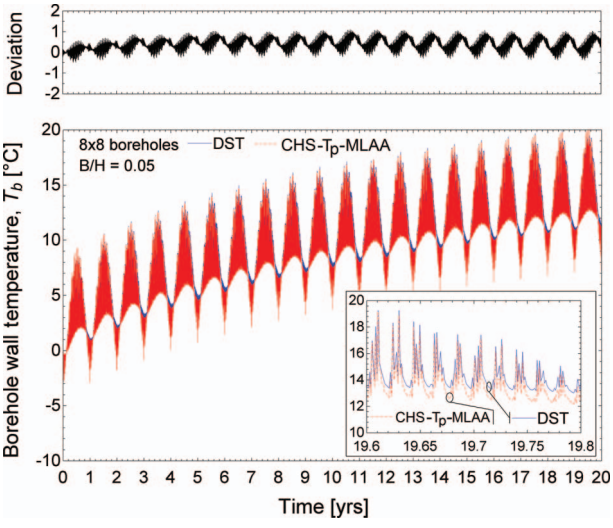

Figure 15. Test MB64-C for 64 boreholes.

8. Conclusion

Several test cases for analytical verification and inter-model comparisons of vertical GHX models are presented in this article. They range from steady-state heat rejection in a single borehole to varying hourly loads with large yearly thermal imbalance in multiple borehole configurations. The usefulness of the proposed test cases is illustrated with different GHX models.

For single boreholes, this comparison exercise has shown that analytical 1D models compare favourably well with 3D models for relatively short-simulation periods, where axial effects are not significant. Results of cyclic heat rejection/collection tests show that the CHS solution compares favourably well with the DST model especially when the non-aggregated time period of the recent loads is large. A synthetic cooling-dominated load profile test case has been used for 20-year simulations. Results show that CHS-based models predict borehole wall temperatures that are well within ± 1°C of the DST model.

A number of tests are also proposed for multiple boreholes. In these tests, three GHX models are compared: DST, *g-function* and the CHS/T_p/MLAA. Constant load tests have shown differences, sometimes large, among these models. These differences are most likely due to two factors. First, the CHS/T_p/MLAA model cannot account for axial effects at the borehole level, which translates into significant differences in the prediction of borehole wall temperatures, especially for long-simulation periods (corresponding to large values of $\ln(t/t_s)$). Second, the limitations of the DST model in terms of bore field configuration have also been pointed out by considering an 8 borehole in-line configuration. Finally, 20-year simulations for a typical load profile and an 8×8 bore field have shown that the hybrid CHS/T_p/MLAA model predicts borehole wall temperature to within 1.1°C of the DST model.

These results show that the proposed test cases are able to identify differences between the models at three levels: local heat transfer (near the borehole), thermal interaction among boreholes and load aggregation. The flexibility of inter-model comparison allows testing models in extreme conditions (e.g. highly imbalanced loads for very long periods of time or rapidly changing heating and cooling loads), and therefore, test different parts of the modelling algorithms. These inter-model comparisons can play a

significant role in discovering modelling errors or selecting appropriate algorithms for a given situation.

It is hoped that this work will help developing a much-needed test and validation suite for GHX models used in energy simulation programs. Other (more complex) test cases can be envisioned to evaluate: (1) moisture migration effects and underground water flows; (2) surface conditions effects (impact of weather conditions); (3) impact of header depth and (4) high-frequency dynamic effects (time steps shorter than 1 h).

Empirical validation is also required to assess the performance of different GHX models and a good set of empirical values would certainly be an asset in the quest for a complete set of validation tools for GHX models.

Nomenclature

Symbol	Unit	Variable
α_g	m^2/day	Ground thermal diffusivity
B	m	Centre-to-centre distance between boreholes
D	m	Borehole header depth
EWT	°C	Entering water temperature
g	–	Eskilon's *g-function*
G	–	CHS solution
H	m	Borehole depth
k_s	W/m-K	Ground thermal conductivity
n	–	Number of boreholes
q	W/m	Heat transfer rate per unit length (negative values for heat rejection into the ground)
Q	W	Heat transfer rate
$\bar{Q}_i$	W	Average heat transfer rate on the ith aggregation period
r_b	m	Borehole radius
t	day	Time
T_b	°C	Borehole wall temperature
T_g	°C	Far-field ground temperature
T_p	°C	Temperature penalty
$T_{\text{in,ground}}$	°C	Bore field inlet fluid temperature
$T_{\text{out,ground}}$	°C	Bore field outlet fluid temperature
t_s	day	Characteristic time
V	m^3	Volume

References

Beier, R.A., Smith, M.D., and Spitler, J.D., 2011. Reference data sets for vertical borehole ground heat exchanger models and thermal response test analysis. *Geothermics*, 40, 79–85.

Bernier, M., Kummert, M., and Bertagnolio, S., 2007. Development and application of test cases for comparing vertical ground heat exchangers. *In*: *Proceedings of the 10th international IBPSA conference*, 3–6 September, Beijing, China, 1462–1468.

Bernier, M.A., 2001. Ground-coupled heat pump system simulation. *ASHRAE Transactions*, 106 (1), 605–616.

Bernier, M.A., 2006. Closed-loop ground-coupled heat pumps systems. *ASHRAE Journal*, 48 (9), 12–19.

Bernier, M.A., Chahla, A., and Pinel, P., 2008. Long-term ground temperature changes in geo-exchange system. *ASHRAE Transactions*, 114 (2), 342–350.

Bernier, M.A., *et al*., 2004. A multiple load aggregation algorithm for annual hourly simulations of GCHP systems. *International Journal of HVAC&R Research*, 10 (4), 471–488.

Carslaw, H.S. and Jaeger, J.C., 1947. *Conduction of heat in solids*. 2nd ed. Oxford: Clarendon Press.

Chapuis, S. and Bernier, M., 2009. Seasonal storage of solar energy in boreholes. *In*: *Proceedings of the 11th international IBPSA conference*, 27–30 July, Glasgow, UK, 599–606.

Cooper, L.Y., 1976. Heating of a cylindrical cavity. *International Journal of Heat and Mass Transfer*, 19, 575–577.

Cui, P., Yang, H., and Fang, Z., 2006. Heat transfer analysis of ground heat exchangers with inclined boreholes. *Applied Thermal Engineering*, 26, 1169–1175.

Eskilson, P., 1987. *Thermal analysis of heat extraction boreholes*. Thesis (PhD). Lund University, Sweden.

Fisher, D.E., *et al*., 2006. Implementation and validation of ground-source heat pump system models in an integrated building system simulation environment. *International Journal of HVAC&R Research*, 12 (3a), 693–710.

Hellström, G., 1991. *Ground heat storage: thermal analysis of duct storage systems*. Thesis (PhD). Lund University, Sweden.

Hellström, G., Mazzarella, L., and Pahud, D., 1996. *Duct ground storage model – TRNSYS version*. Sweden: Department of Mathematical Physics, University of Lund.

Hern, S.A., 2002. *Design of an experimental facility for hybrid ground source heat pump systems*. Thesis (MSc). Oklahoma State University, USA.

Huber, A. and Pahud, D., 1999. *Erweiterung des Programms EWS für Erdwärmesondenfelder*, Bundesamt für Energie.

Ingersoll, L.R. and Plass, H.J., 1948. Theory of the ground pipe heat source for the heat pump. *Heating, Piping and Air Conditioning*, 20, 119–122.

Ingersoll, L.R., Zobel, O.J., and Ingersoll, A.C., 1954. *Heat conduction: with engineering and geological applications*. 2nd ed. New York: McGraw-Hill.

Judkoff, R. and Neymark, J., 1995. *IEA-BESTEST and diagnostic method*. Golden, CO: NREL.

Kelvin, K., Larmor, J., and Joule, J., 1882. *Mathematical and physical paper*. Cambridge: Cambridge University Press.

Klein, S.A., 2006. *TRNSYS. A transient simulation program*. Madison, WI: Solar Energy Laboratory, University of Wisconsin.

Philippe, M., Bernier, M., and Marchio, D., 2009. Validity ranges of three analytical solutions to heat transfer in the vicinity of single boreholes. *Geothermics*, 38, 407–413.

Piechowski, M., 1998. Heat and mass transfer model of a ground heat exchanger: validation and sensitivity analysis. *International Journal of Energy Research*, 22, 965–979.

Reuss, M., Beck, M., and Müller, J.P., 1997. Design of a seasonal thermal energy storage in the ground. *Solar Energy*, 59, 247–257.

Shonder, J.A., Baxter, V., and Thornton, J.W., 1999. A new comparison of vertical ground heat exchanger design methods for residential applications. *ASHRAE Transactions*, 105 (2), 1179–1188.

Shonder, J.A., *et al*., 2000. A comparison of vertical ground heat exchanger design software for commercial applications. *ASHRAE Transactions*, 106 (1), 831–842.

Spitler, J.D., *et al*., 2009. Preliminary intermodel comparison of ground heat exchanger simulation models. *In*: *Proceedings of the Effstock conference*, 14–17 June, Stockholm, Sweden, paper #115, 8.

Tarnawski, V.R. and Leong, W.H., 1993. Computer analysis, design and simulation of horizontal ground heat exchangers. *International Journal of Energy Research*, 17, 467–477.

Yavuzturk, C. and Spitler, J.D., 1999. A short time step response factor model for vertical ground loop heat exchangers. *ASHRAE Transactions*, 105 (2), 475–485.

Yavuzturk, C., and Spitler, J.D., 2001. Field validation of a short time-step model for vertical ground-loop heat exchangers. *ASHRAE Transactions*, 107 (1), 617–625.

Yu, Y., Ma, Z., and Li, X., 2008. A new integrated system with cooling storage in soil and ground-coupled heat pump. *Applied Thermal Engineering*, 28, 1450–1462.

Zeng, H., Diao, N., and Fang, Z., 2002. A finite line-source model for boreholes in geothermal heat exchangers. *Heat Transfer-Asian Research*, 31 (7), 558–567.

Appendix 1

The synthetic profiles shown in Figures 8 and 10 are obtained using the following mathematical function:

$$y = f(t, A, B, C) + (-1)^{FL} \times abs\{f(t, A, B, C)\} + D \times (-1)^{FL} \times SN$$

where

$$f(t, A, B, C) = A \times \sin\left(\frac{\pi \times (t - B)}{12}\right) \times \sin\left(\frac{F \times \pi \times (t - B)}{8760}\right) \times \left[\frac{168 - C}{168} + \sum_{i=1}^{3} \frac{\left(\cos\left(\frac{i \times \pi \times C}{84}\right) - 1\right) \times \sin\left(\frac{i \times \pi \times (t-B)}{84}\right)}{i \times \pi}\right],$$

$$FL = floor\left(\frac{F \times (t - B)}{8760}\right),$$

and

$$SN = signum\left(\cos\left(\frac{F \times \pi \times (t + G)}{4380}\right) + E\right).$$

In the above equations, y is the load, angles are measured in radians, t is the time variable, '*floor*' is the largest integer less than or equal to the number considered, '*abs*' denotes the absolute value of the expression and '*signum*' is equal to plus or minus one according to the sign of the expression evaluated. The synthetic asymmetric profile, as shown in Figure 8, was obtained using the following parameters: $A = 2000$, $B = 1000$, $C = 80$, $D = 0.01$, $E = 0.95$, $F = 4/3$ and $G = 2190$. The symmetric profile used to generate the loads shown in Figure 10 was obtained using the following parameters: $A = 2000$, $B = 2190$, $C = 80$, $D = 0.01$, $E = 0.95$, $F = 2$ and $G = 0$.